

Mapping coastal erosion at the Nile Delta western promontory using Landsat imagery

Mohamed E. Hereher

Received: 17 May 2010 / Accepted: 12 January 2011 / Published online: 28 January 2011
© Springer-Verlag 2011

Abstract A set of six Landsat satellite images with 5–9 years apart was used in a post-classification analysis to map changes occurred at Rosetta promontory between 1973 and 2008 due to coastal erosion. Spectral information were extracted from two multi-spectral scanner (MSS) images (1973 and 1978), three thematic mapper (TM) images (1984, 1990, and 1999), and one enhanced thematic mapper plus (ETM+) image (2008). To estimate the quantity of land loss in terms of coastal erosion, a supervised classification scheme was applied to each image to highlight only two classes: seawater and land. The area of each class was then estimated from the number of pixels pertaining to this class in every image. In addition, the shoreline position was digitized to address retreat/advance pattern throughout the study period. Results showed that Rosetta promontory had lost 12.29 km² of land between 1973 and 2008 and the shoreline withdrew southward about 3.5 km due to coastal erosion. Most land loss and shoreline retreat occurred between 1973 and 1978 (0.55 km²/year and 132 m/year, respectively). Coastal protection structures were constructed successively at the promontory. These structures have considerably contributed to reduce coastal erosion; however, they promoted downdrift erosion.

Keywords Coastal erosion · Change detection · Remote sensing · Rosetta

Introduction

Satellite data can afford a synoptic view with a wide geographic coverage, periodic imaging of the same region and multiple spectral information ranging from the visible to the infrared portions of the spectrum. The launch of Landsat satellite in 1972 provided an invaluable historical digital record of marine and terrestrial ecosystems. The unique interaction between water bodies and electromagnetic radiation (EMR), in which seawater absorbs more EMR than any other terrestrial landscape (Lillesand and Kiefer 2000), makes water bodies easily distinguished from contiguous coastal land masses. Satellite images could address and map these changes.

Change detection is the process of identifying differences in the status of an object by observing it at different dates (Singh 1989). Change detection of satellite data ranges from visual comparison to complex image processing schemes. Common change detection techniques include simple band ratio, principal component analysis, vegetation index algorithms, and others. Major data sources include MSS, TM, ETM+, Systeme Pour l'Observation de la Terre (SPOT), moderate resolution imaging spectroradiometer (MODIS), advanced very high resolution radiometer (AVHRR), and other sensors. Post-classification change detection is a famous technique applied to address thematic changes in satellite data. The advantage of using this approach is its application to data from different sensors with high degree of confidence (Song et al. 2001). In addition, post-classification comparison proved to be effective technique, because data from two or more dates are independently classified, thereby minimizing problems arising from atmospheric correction (Shalaby and Tateishi 2007) and/or sensor degradation.

M. E. Hereher (✉)
Department of Environmental Sciences,
Faculty of Science at Damietta, Mansoura University,
New Damietta, Egypt
e-mail: mhereher@yahoo.com

The study area

The present Nile Delta has two promontories: the eastern is at Damietta and the western is at Rosetta. At these two promontories, the River Nile ends its journey which exceeds 6,000 km long. The present study focuses on the western promontory of the Nile Delta, i.e., Rosetta (Fig. 1). The evolution of Rosetta promontory is discussed in Frihy and Lawrence (2004). Generally, the promontory is a costal headland with flat terrain covered by sand mounds and small sand dunes. The beach is composed of fine to very fine quartz sand and rich in heavy minerals (Frihy et al. 1994). There are many low-laying areas forming salt-crusted sabkhas. The headland is inundated periodically by seawater during winter sea surges. Agricultural lands encompass the River Nile course. Urban areas include the city of Rosetta along with many other small villages. The climate of the region is generally Mediterranean. Precipitation occurs during winter and approaching 200 mm annually. Temperature is mild with maximal temperature in August (27°C) and minimal in January (14°C). Due to its proximity to the Mediterranean Sea, the relative humidity is generally high (72% in summer). Wind blows mostly from the northwestern (NW) direction. The trend of wind creates a general west-to-east nearshore current (mainly a longshore current) moving parallel to the coast. This current dominates the entire delta coast and carries eroded sediments eastward where they deposit along any receiving embayment or saddles.

The phenomenon of coastal erosion along the delta promontories started at the early 1900s after constructing

the Aswan Low Dam (Sestini 1992). The problem was triggered after the closure of Aswan High Dam in 1964. The majority of research carried out upon monitoring coastal erosion at the delta promontories, particularly Rosetta was extracted from topographic maps, aerial photographs, and beach profile studies. Few studies were carried out using satellite remote sensing. Elsayed and Mahmoud (2007) mentioned that the shoreline retreat at Rosetta was estimated at 20 m/year between 1941 and 1964. This rate was accelerated to 120 m/year after 1964 until 1990 as the result of the closure of the Aswan High Dam. El-Fishawi (1989) reported that Rosetta headland lost 14.7 km² between 1909 and 1988. Blodget et al. (1991) used MSS data to monitor the shoreline at Rosetta region between 1972 and 1987. They concluded that Rosetta area is subjected to both degradation and aggradation processes during the 15 years of study. Frihy et al. (1994) conducted a shoreline change study using MSS images between 1972 and 1991 and observed that the headland retreat rate approached 71 m/year. The objective of the present study is to update and address the change occurred at Rosetta headland until 2008 taking into account the impact of the constructed coastal protection measures upon erosion/accretion patterns.

Materials and methods

Data set

In order to track the shoreline position change at Rosetta promontory, a series of Landsat satellite images was used

Fig. 1 Location map of Rosetta promontory showing the headland geomorphology



Table 1 Satellite data utilized in the present study

Sensor	Acquisition date	Path/row	Pixel size (m)
MSS	May 1973	190/38	60
MSS	May 1978	190/38	60
TM	September 1984	177/38	30
TM	August 1990	177/38	30
TM	February 1999	177/38	30
ETM+	July 2008	177/38	30
SRTM	February 2000	177/38	90

in this study (Table 1). This group includes images from the MSS (1973 and 1978), TM (1984, 1990 and 1999), and ETM+ (2008) sensors. Satellite data were acquired at no cost from the United States Geological Survey (USGS) on-line open resources (<http://edcscns17.cr.usgs.gov/Earth Explorer>). As there was a lot of change along Rosetta headland during the past three decades, it was important to have an appropriate time interval (5–9 years) between each two consecutive images. The available images were of high quality as they were mostly free from clouds. The only exception was the ETM+ image of 2008 which had a sensor scan-line problem. The spatial resolution is 60 m for the MSS images and 30 m for both the TM and ETM+ images. All images were acquired in the summer season except the TM image of 1999 which was taken during winter. At this time of the year, i.e., winter, the headland is usually flooded by seawater for a few weeks and water extends inland for several kilometers. The spectral information utilized in this study comprises four bands from the MSS images (two in the visible and two in the infrared spectrum) and six bands from both the TM and ETM+ images (three in the visible and three in the infrared spectrum). In addition, a digital elevation model (DEM) from the shuttle radar topography mission (SRTM) acquired in February 2000 with a 90 m spatial resolution was used to analyze the topography of the region. This image was acquired from the global land cover facility (GLCF) web portal (<http://www.landcover.org/index.shtml>).

Image preprocessing

All image processing procedures were applied using ERDAS Imagine and ArcGIS Software packages. Figure 2 summarizes processing steps applied to satellite data. Image geometric correction was applied first to all images. Although the acquired images were originally rectified, it was better to reproject the image set using topographic maps and ground control points (GCPs). The most recent topographic map (1:50,000) of Rosetta region drawn from aerial photographs of the years 1990–1991 was used as the base map to rectify the satellite TM image of 1990 through

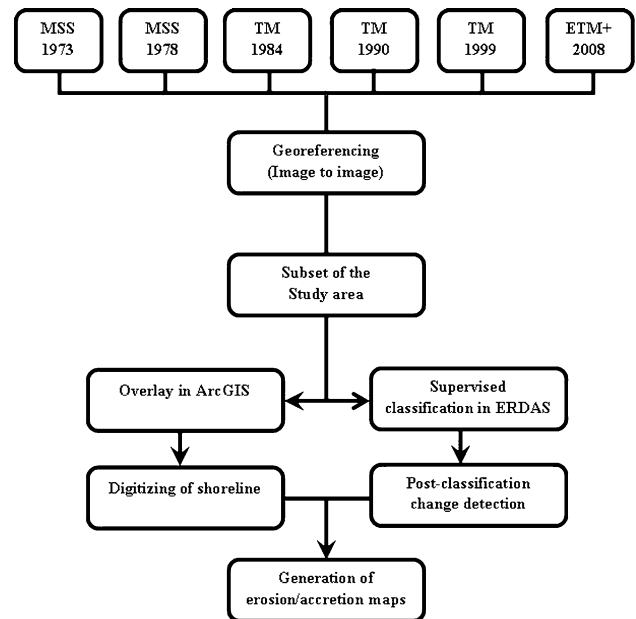


Fig. 2 Flow-chart diagram showing the image processing steps applied in the study

image to map rectification. A total of 25 prominent points were selected and a first order polynomial transform was applied. Other ground points were selected at well-known features using a GPS at the intersection of major roads and canals. It was important to acquire the coordinates of renowned features as appear in the map and in the field. After rectification, the image of 1990 was considered as the master image from which the other images were georeferenced to the Universal Transverse Mercator (UTM—WGS 84—Zone 36 N) projection through image to image rectification. It was crucial to have a low error of rectification as low as one pixel at most. To make an accurate change detection using the MSS, TM, and ETM+ images, the two MSS images, which have a spatial resolution of 60 m were resampled to 30 m pixel size, so that all the satellite images have the same spatial resolution (30 m). Although Song et al. (2001) mentioned that atmospheric correction is not necessary when images are to be classified independently, simple dark object subtraction (Chavez 1996) was applied in order to eliminate any atmospheric interference caused by haze or aerosols. The dark object used was the clean deep seawater of the Mediterranean Sea north of the study area. However, there was no need to carry out further radiometric normalization as the classified images were acquired in the same season except the 1999 TM image.

Image classification

One of the most important applications of satellite remote sensing is land cover classification. Although there are

many land cover units present in the study area, such as agricultural land, urban areas, coastal plain, the Nile River, and the Mediterranean Sea (Fig. 1), the objective of classification process was to group all terrestrial units together and separate them from all aquatic units so that there are only two supervised classes; land and water. Consequently, any loss of the total area of land between two images represents erosion. Training well-known sites based on the field trips and spectral signatures of land and water at the region were used to identify each class. To make a suitable classification, all the spectral bands within the MSS, TM, and ETM+ images, except the thermal bands, have been utilized in the classification process. A supervised classification using maximum likelihood classifier (MLC) algorithm was applied to perform final classification based on the probability of a pixel belonging to each class. Each classified image was then recoded into land and water. The area of land was then calculated in each image. The ETM+ image of 2008 which has a scan-line problem causing apparent lines in the classified image was treated in order to correct the errors caused by these lines. In ERDAS Imagine Modeler, a model was created to amend and convert pixels present in the bad scan-line to the corresponding actual class, either water or land. The classified images were then refined using 3×3 majority filters to remove odd pixels in the classified matrix. In addition, the DEM of the region was classified in ArcGIS to yield two classes: below sea level (≤ 0.0 m) and above sea level (> 0.0 m) in order to highlight low-land areas at the promontory.

Accuracy assessment

Although there were only two land cover units in each map; land and water, it was necessary to make an accuracy test for classification. A total of 50 random pixels were selected at each land cover map using the stratified random approach and compared with the original pixels in the corresponding images. A careful pixel to pixel check was applied. In addition, a topographic map drawn from aerial photographs during 1990–1991 was used as an independent reference for accuracy assessment of the 1990 land cover map. Field excursions during 2009 were carried out to survey the region and to track the shoreline position at many locations using a GPS instrument. The user accuracy, producer accuracy, and Kappa statistics were calculated.

Change detection

Post-classification is one approach of land use/land cover change detection (Singh 1989). One important advantage of post-classification change detection is that the images are classified separately which minimizes the problem of radiometric normalization between dates and lowers the

amount of pre-processing work (Song et al. 2001 and Wang et al. 2009). The post-classification change detection provides the “from-to” information, which can be used to define the magnitude and location of the land cover transformation from thematic data (Yuan et al. 2005). This kind of classification is the most widely used for identifying land use and land cover change (Lu et al. 2004). However, accuracy of this approach is as good as the classification accuracy of each land cover map. Post-classification change detection was applied in numerous studies (e.g., Mas 1999; Coppin et al. 2004; Dewan and Yamaguchi 2009). In the present study, the change of the total land area from each classified image was estimated and the change matrix was obtained. In addition, a cross tabulation analysis was applied in order to estimate the “from-to” transformation between land and water at the very early and very late land cover maps, i.e., 1973 and 2008. Finally, the shoreline position change at the promontory was digitized in ArcGIS to delineate the advance and retreat trajectories detected in the six satellite images between 1973 and 2008.

Results and discussion

The accuracy assessment of all land cover maps approached 100% for the producer and user accuracies as well as for the overall accuracy. Moreover, Kappa statistics coefficient is 1.0 for water and land classes meaning that the classification process was accurate. Figure 3 shows the six images of the study area, the corresponding classified images and the total land area at each date. Table 2 represents the change in land area and shoreline retreat. The promontory land area is estimated from satellite images at 74.91 km² in 1973, 71.56 km² in 1978, 69.26 km² in 1984, 67.64 km² in 1990, 63 km² in 1999, and 62.62 km² in 2008. Maximum land loss rate (erosion) occurred during 1973–1978 (0.55 km²/year), whereas the minimum occurred during 1999–2008 (0.03 km²/year) due to the construction of integrated coastal protection system. Significant erosion was encountered during 1978–1984, and during 1990–1999 (0.46 km²/year for both). The total land loss between 1973 and 2008 is 12.29 km² with a mean annual rate of 0.34 km²/year. Figure 4 highlights the locations of erosion and accretion along the promontory from which it is clear that the headland was the location witnessed maximal erosion. Eroded sediments were transported by the eastward longshore currents and deposited east of the promontory. Figure 5 represents the locations of the shoreline at each date. Successive retreat is observed along the headland and at the western side of the promontory. On the other hand, shoreline advance is observed east of the promontory due to accretion. Utmost retreat occurred along the headland between 1973 and 1978

Fig. 3 The six row subset images of Rosetta, the corresponding classified images and the land area at each date

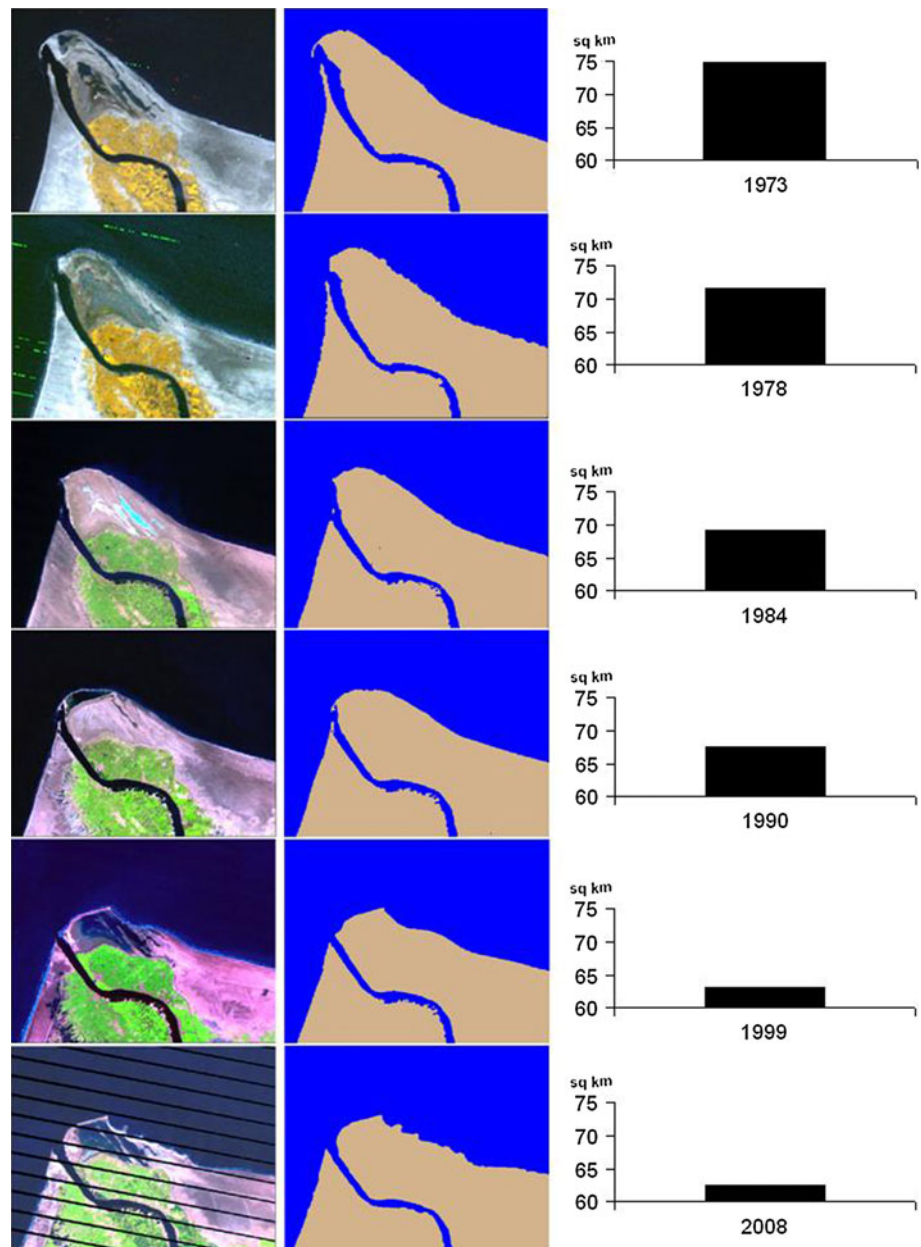


Table 2 Land loss and shoreline retreat at Rosetta between 1973 and 2008

Year	Land loss (km ²)	Loss rate (km ² /year)	Shoreline retreat (m)	Retreat rate (m/year)
1973–1978	−3.35	0.55	791	132
1978–1984	−2.3	0.46	889	127
1984–1990	−1.62	0.23	695	99
1990–1999	−4.64	0.46	788	79
1999–2008	−0.38	0.03	313 ^a	31 ^a
1973–2008	−12.29	0.34	3,476	96

^a Measurements were done at the western side of the promontory

(791 m). However, after constructing the eastern and western revetments (seawall) no further withdraw occurred at the headland, though other unprotected shores have suffered from erosion. Figure 6 shows the topography of the region as extracted from the only available coarse resolution (90 m) DEM. Substantial area is located below the sea level, particularly near the headland. These lowland areas are occasionally exposed to flooding during winter surges and consequently triggering land degradation. Results of the present study are a bit different from the earlier studies as most previous investigations extract shoreline locations from topographic maps and aerial photographs. Little

Fig. 4 Locations of accretion and erosion areas at Rosetta promontory

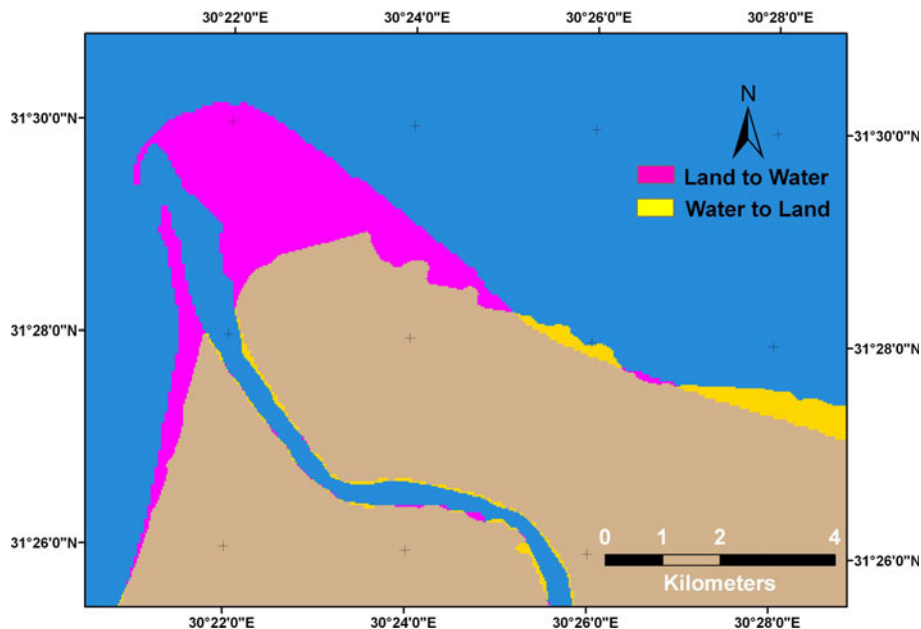
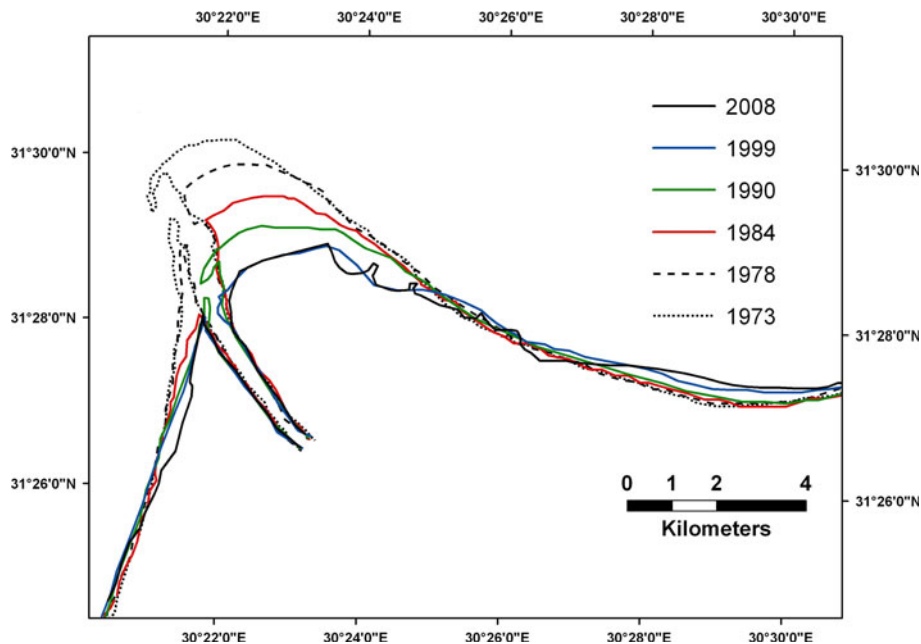


Fig. 5 Shoreline position at Rosetta promontory at the six dates of study



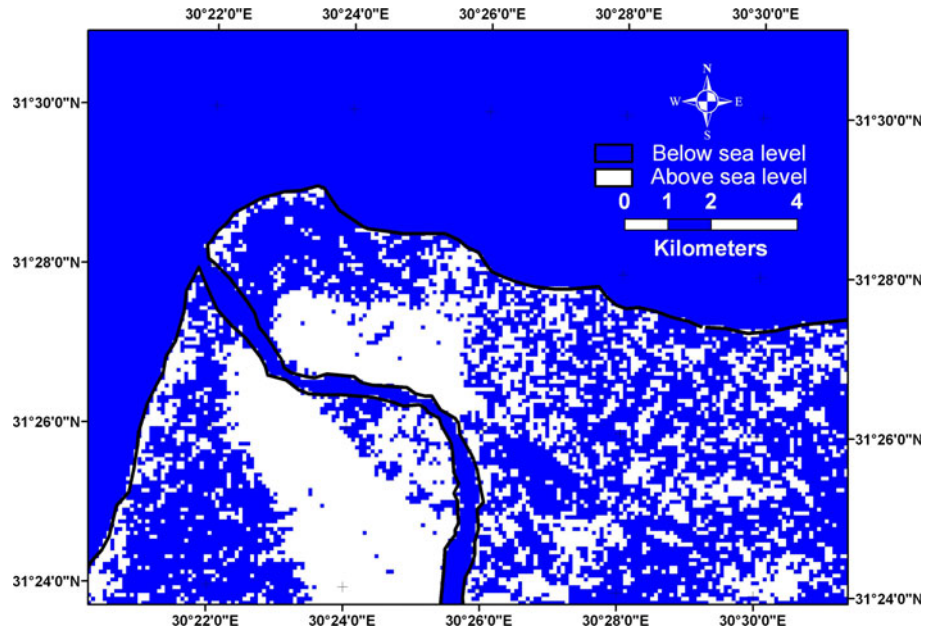
previous studies utilized relatively high resolution satellite data as used in this study.

Driving forces of change

The Nile Delta is considered a wave-dominant delta (Coleman et al. 1981) after a short historic constructive phase during the Holocene (Said 1993). Frihy et al. (2003) reported that the main wave directions along the Nile Delta coast are from the N–W and N–E quadrants, with a predominance of the N–W directions (81%). This wave trend creates a N–E longshore current parallel to the coast.

Maximum wave height recorded at Rosetta approached 5.4 m during 1988 (Frihy et al. 2008). It was reported that about 90 million tons of sediments were discharged annually in the past into the Mediterranean Sea via Rosetta (65%) and Damietta (35%) branches (Sestini 1992). Between 1800 and 1900, the Nile Delta headlands (Rosetta and Damietta) extended seaward by 3.6 and 3.0 km, respectively (McManus 2002). The construction of the dams and water control works along the River Nile course had diminished this annual sediment discharge, which in turn triggered the phenomenon of coastal erosion. For example, the construction of the delta barrages had resulted

Fig. 6 Digital elevation model classified image showing the topography of Rosetta promontory



in coastal erosion of Rosetta by 20 m/year during the period 1941–1964 (Elsayed and Mahmoud 2007). After the closure of the Aswan High Dam during 1964, all the sediments were deprived from reaching the Mediterranean Sea shore and the problem was noticeable at the delta headlands (Rosetta at the west, Burullus at the middle, and Damietta at the east). The present study shows that the onset of shoreline retreat at Rosetta promontory was great during the 1970s and 1980s (132 m/year and 127 m/year during 1973–1978 and 1978–1984, respectively). This rate is comparable to some previous estimates at the region (80–120 m/year between 1970 and 1987, Frihy 1988). The rate of erosion at the headland was significantly lowered due to the construction of two seawalls along the eastern and western margins of the headland during 1986–1987, however, coastal erosion was observed afterwards at the unprotected beaches.

The role of protection measures

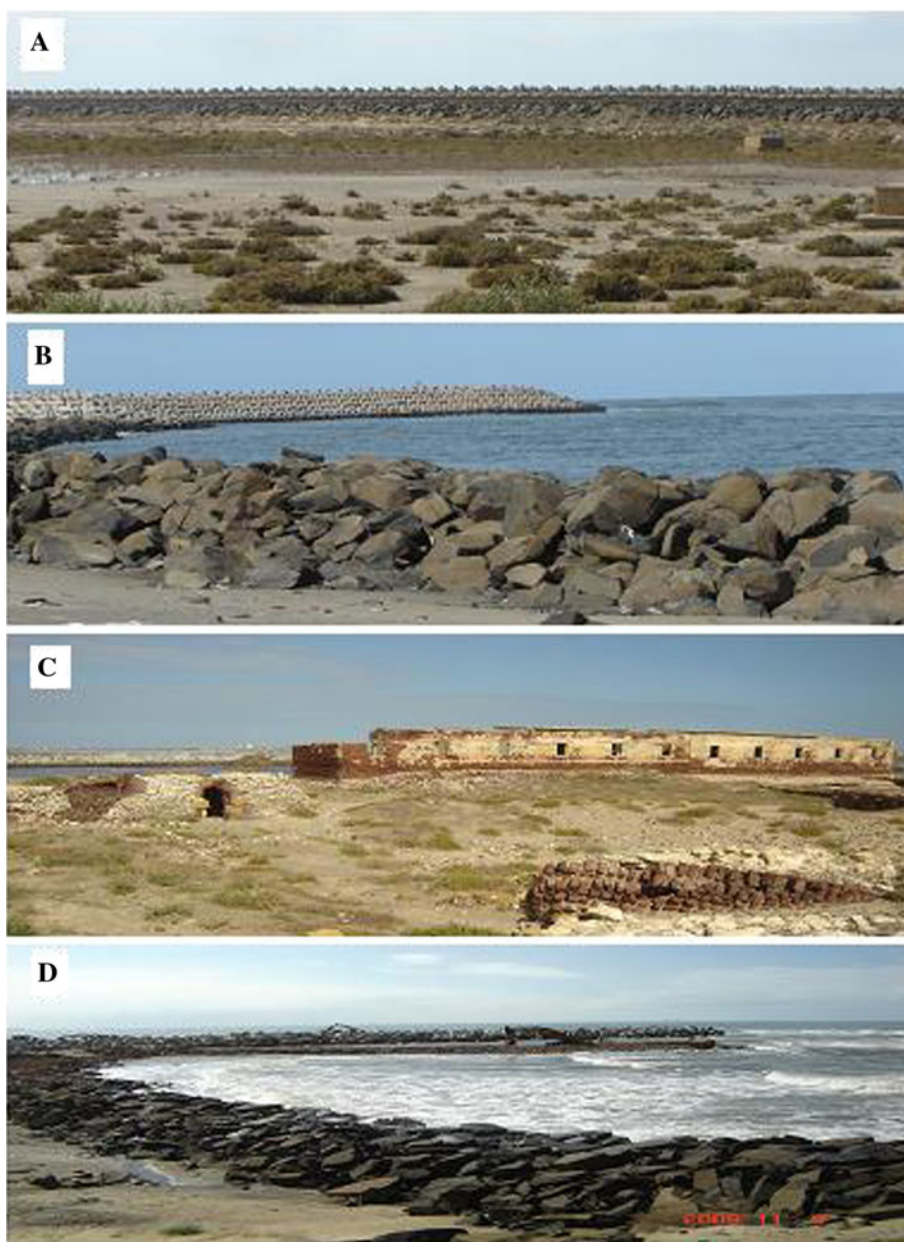
Two seawall revetments of dolos concrete blocks were constructed by the Egyptian Shore Protection Authority to protect Rosetta headland from erosion (Fig. 7a, b). The western revetment (1.5 km long) was constructed during 1986–1991 and the eastern revetment (3.5 km long) was constructed during 1988–1991 (Elsayed et al. 2005). Although these seawall revetments were effective to prevent further headland loss, they caused erosion at the upside and downside ends of these seawalls. This is translated to a loss of 4.64 km² during the period (1990–1999) (Table 2). Maximum erosion occurred at the eastern side of the promontory. In order to protect this eastern side, a field of 5 groins (400–500 m length) was constructed seaward during

2003 with 800–900 m spacing along the shoreline (Dewidar and Frihy 2007). Consequently, the land loss rate was diminished to only 0.38 km² between 1999 and 2008 (Table 2). On the other hand at the updrift end of the western revetment, some archeological sites were vulnerable to threat by erosion (Fig. 7c). At this location, the shoreline retreated 313 m between 1999 and 2008 (Table 2). New protection measures at this site are being implemented by a new groin filed as well as basaltic seawalls (Fig. 7d).

The impact of sea-level rise and land subsidence

Generally, changes at coastal areas intimately affect socio-economic attitudes of humans. Mikhailova (2001) mentioned that the main factors contributing to the washout of the coastline of the Nile Delta are the human-induced cut-off of sediment discharge through the River Nile, sea waves, eustatic sea-level rise, and land subsidence. Viewing the topography of the study area (Fig. 6), it is clear that substantial area lies below the sea-level. This area is periodically inundated during winter; consequently, a little rise in the sea-level will accelerate coastal erosion and seriously affect any land use in the region. The rate of sea level rise was estimated at Alexandria (about 60 km west of Rosetta) by 2 mm/year between 1944 and 1989 (Frihy 1992). The rise in the sea level by 100 cm will inundate about 30% of the Nile Delta including Rosetta headland (Hereher 2010). In addition, it was reported that the Nile Delta is experiencing regional subsidence ranging from 0.1–0.25 cm near Alexandria at the west up to 0.5 cm near Port Said at the east (Stanley 1990). The situation will be worse if the eustatic sea-level rise is coupled with the regional subsidence of the coastal land. These factors and

Fig. 7 **a, b** shows the western seawall revetment, **c** shows an archeological fort vulnerable to flooding, and **d** shows the new basaltic sea wall near the historical buildings



others lead Stanley and Warne (1998) to claim that the Nile Delta is in its destructive phase.

Conclusions

Mapping coastal change using satellite remote sensing asserts on the advantage of using this tool over the tedious routine ground survey. However, field truthing is an indispensable task to verify remotely sensed data. In addition, radar imaging has broadened the scope of investigation for an integrated perspective. The main conclusion of this study is that the headland of Rosetta promontory witnessed severe coastal erosion between 1973

and 2008. This environmental change is a direct human-induced intervention by damming along the Nile River course. Although coastal protection works helped protect the coast, they have some erosion consequences along their margins and at their downdrift sides. Due to its low land level, the study area is susceptible to eustatic sea-level rise. This inundation could be triggered by regional subsidence.

References

- Blodget H, Taylor PT, Roak JH (1991) Shoreline changes along the Rosetta-Nile Promontory: monitoring with satellite observations. *Marine Geol* 99:67–77

- Chavez PS (1996) Image-based atmospheric correction—revised and improved. *Photogram Eng Remote Sens* 62:1025–1036
- Coleman JM, Robert HH, Murray SP, Salama M (1981) Morphology and dynamic sedimentology of the eastern Nile delta shelf. *Marine Geol* 42:301–312
- Coppin P, Jonckheer I, Nackarts K, Muys B, Lambin E (2004) Digital change detection methods in ecosystem monitoring: a review. *Int J Rem Sens* 25:1565–1596
- Dewan AM, Yamaguchi Y (2009) Land use and land cover change in Greater Dhaka, Bangladesh: using remote sensing to promote sustainable urbanization. *Appl Geogr* 29:390–401
- Dewidar Kh, Frihy OE (2007) Pre- and post-beach response to engineering hard structures using Landsat time-series at the northwestern part of the Nile delta, Egypt. *J Coast Conserv* 11:133–142
- Elsayed MA, Mahmoud S (2007) Groins System for Shoreline Stabilization on the East Side of the Rosetta Promontory, Nile Delta Coast. *J Coast Res* 23:380–387
- Elsayed MA, Younan NA, Fanos AM, Baghdady KH (2005) Accretion and erosion patterns along Rosetta promontory, Nile Delta coast. *J Coast Res* 21:412–420
- El-Fishawi NM (1989) Coastal erosion in relation to sea level changes, subsidence and river discharge, Nile Delta coast. *Acta Mineralogica Petrograph* 30:161–171
- Frihy OE, Nasr SM, El Hattab MM, El Raey M (1994) Remote sensing of beach erosion along the rosetta promontory, north-western Nile delta, Egypt. *Int J Rem Sens* 15:1649–1660
- Frihy OE (1988) Nile Delta shoreline changes: aerial photographic study of a 28-year period. *J Coast Res* 4:597–606
- Frihy OE (1992) Sea-level rise and shoreline retreat of the Nile Delta Promontories, Egypt. *Nat Hazards* 5:65–81
- Frihy OE, Lawrence D (2004) Evolution of the modern Nile delta promontories: development of accretional features during shoreline retreat. *Environ Geol* 46:914–931
- Frihy OE, Debes EA, El Sayed WR (2003) Processes reshaping the Nile delta promontories of Egypt: pre- and post-protection. *Geomorphology* 53:263–279
- Frihy OE, Shereet SM, El Banna MM (2008) Pattern of beach erosion and scour depth along the Rosetta Promontory and their effect on the existing protection works, Nile Delta, Egypt. *J Coast Res* 24:857–866
- Hereher M (2010) Vulnerability of the Nile Delta to sea level rise: an assessment using remote sensing. *Geomat Nat Hazards Risk* 1(4):315–321
- Lillesand MT, Kiefer RW (2000) Remote sensing and image interpretation. John Wiley & Sons Inc., New York
- Lu D, Mausel P, Brondizio E, Moran E (2004) Change detection techniques. *Int J Rem Sens* 25:2365–2407
- Mas JF (1999) Monitoring land-cover changes: a comparison of change detection techniques. *Int J Rem Sens* 20:139–152
- McManus J (2002) Deltaic responses to changes in river regimes. *Mar Chem* 79:155–170
- Mikhailova MV (2001) Hydrological regime of the Nile delta and dynamics of its coastline. *Water Res* 28:477–490
- Said R (1993) The River Nile. Geology, hydrology and utilization. Pergamon Press, Oxford, p 320
- Sestini G (1992) Implications of climatic changes for the Nile Delta. In: Jeftic L, Milliman D, Sestini G (eds) Climatic change and the mediterranean. Edward Arnold, London, pp 535–601
- Shalaby A, Tateishi R (2007) Remote sensing and GIS for mapping and monitoring land cover and land-use changes in the Northwestern coastal zone of Egypt. *Appl Geogr* 27:28–41
- Singh A (1989) Digital change detection techniques using remotely sensed data. *Int J Rem Sens* 10:989–1003
- Song C, Woodcock CE, Seto KC, Lenney MP, Macomber SA (2001) Classification and change detection using Landsat TM data: when and how to correct atmospheric effects. *Rem Sens Environ* 75:230–244
- Stanley DJ (1990) Recent subsidence and northeast tilting of the Nile delta, Egypt. *Marine Geol* 94:147–154
- Stanley DJ, Warne AG (1998) Nile delta in its destruction phase. *J Coast Res* 14:794–825
- Wang Y, Brian R, Mitchell BM, Marzilli JN, Bonygne G, Zhou Y, Shriver G (2009) Remote sensing of land-cover change and landscape context of the National Parks: a case study of the Northeast Temperate Network. *Rem Sens Environ* 113:1453–1461
- Yuan F, Sawaya KE, Loeffelholz BC, Bauer ME (2005) Land cover classification and change analysis of the Twin Cities (Minnesota) metropolitan area by multitemporal Landsat remote sensing. *Rem Sens Environ* 98:317–328